JOURNAL OF MATERIALS SCIENCE 8 (1973) 1482-1494

Precipitation in liquid-quenched Al-base Ag alloys

R. ROBERGE
IREQ, Institut de recherche de l'Hydro-Québec, Varennes, Québec, Canada
H. HERMAN
Department of Materials Science, State University of New York at Stony Brook, Stony Brook, Long Island, New York, USA

Al-base Ag alloys have been quenched from the liquid state and aged at temperatures within the metastable miscibility gap. It is found that in the liquid-quenched condition the alloys contain a solute cluster size-distribution which is considerably narrower than that obtained by normal bulk-quenching. Indeed, liquid-quenching is far more effective than fast bulk-quenching in minimizing clustering. Electrical resistivity, wide-angle and small-angle X-ray techniques and transmission electron microscopy have been used to study the evolution of the decomposition products on ageing the liquid-quenched alloys.

1. Introduction

Phase decomposition in quenched Al-base Ag alloys has been the object of numerous studies [1]. Small-angle X-ray scattering (SAXS) and electrical resistivity measurements carried out during ageing near ambient temperature have been interpreted in terms of a high density (10^{18} cm^{-3}) of GP zones which form at the observed high rates owing to enhanced diffusion resulting from excess quenched-in vacancies.

Several detailed models have been proposed for the structure and distribution of GP zones. A study by Baur and Gerold [2] established that the concentration of silver in the zones is controlled by a metastable miscibility gap which is totally submerged within the equilibrium two-phase region (Fig. 1). The gap is asymmetric and exhibits a constriction in the temperature range 140 to 200°C. Of further interest is the fact that for a considerable composition range the gap is inaccessible by solid quenching: the gap ranges from 0 to 60 at. % Ag, while the high-temperature single-phase region which is available for solution treatment extends only to 23 at. % Ag.

Quenching speed is of central importance in order to preserve a solid solution, the decomposition of which is to be studied. This is particularly true in Al-base Ag since the metastable gap has a critical temperature of 450°C, which is only 70°C below the solvus line. The speed and technique of solid quenching have improved considerably over the years, but it has not been possible to avoid solute clustering during the quench. *Liquid quenching*, in addition to enabling an exceedingly fast cooling rate ($\sim 10^6$ °C sec^{-1}), permits the formation of metastable decomposition products in regions of the phase diagram which could not be attained by solid quenching. Furthermore, liquid quenching has frequently led to significant extension of solid solubility, new crystalline phases have been observed, and under certain circumstances amorphous phases are formed. Several reviews of liquid quenching have been published [3-7].

The main objectives of the present study are two-fold: (1) to quench into a region of the phase diagram not accessible by solid-quenching methods; (2) to quench at ultrahigh rates in order to obtain the most random solid solution possible. Electrical resistivity, X-ray techniques and transmission electron microscopy were used to characterize the as-quenched condition and to follow the rates of formation, the structures and the morphologies of the evolving decomposition products.

2. Experimental procedure

Master alloys of each composition, 20, 40, 60, 70.5 and 80 % Ag, weighing approximately 200 g, were prepared from 4N silver powder and 5N

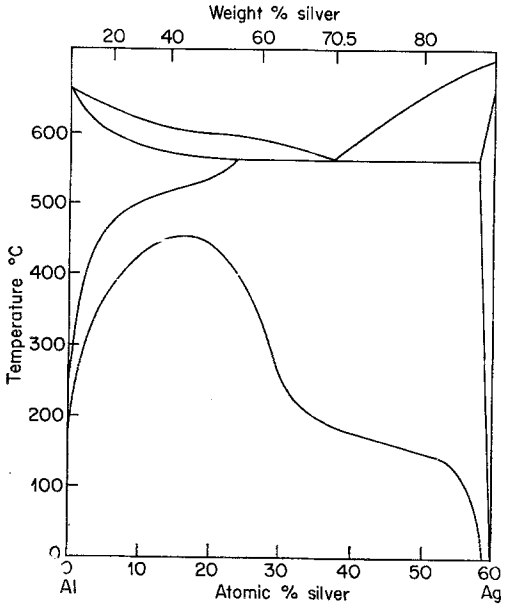

Figure 1 Al-Ag phase diagram showing the metastable miscibility gap. [Baur and Gerold, *Acta Metallurgica* **10** (1962) 637].

aluminium rods (A. D. Mackay, Inc.)*. The alloys were melted under argon in an induction furnace.

Liquid quenching was carried out using two different methods. The device known as the *torsion-catapult* has been described previously [8], and consists in catapulting (at subsonic velocities) the melt out of a curved furnace against a copper substrate. In addition, a device similar in principle to the original *gun technique* of Duwez [9] was also used.

In a few cases, to illustrate the difference between solid quenching and liquid quenching, some of the liquid-quenched specimens were re-homogenized in the single phase region and solid-quenched. The solution treatment was carried out in 550°C molten salt, and the specimens were quenched manually into 25°C water. For all isothermal ageing the specimens were immersed in silicone oil controlled to $\pm$ 0.05°C.

For X-ray studies, Debye-Scherrer patterns were taken in an 11.46 cm diameter camera, using Ni-filtered Cu radiation (40 kV and 26 mA) with exposures for 4 h. Diffractometer measurements were taken using copper radiation (45 kV and 15 mA), monochromatized by a LiF crystal in conjunction with a pulse height analyser.

For transmission electron microscopy (TEM), no thinning was necessary in the case of the liquid-quenched specimens obtained by the gun technique. Some flakes were sufficiently transparent to electrons. The edges of the torsion-catapult foils were also directly usable for transmission.

Electrical resistance of the specimens was measured by the potentiometric four-probe method. An interruption technique was used for measurements, the resistance being determined at 20°C in a temperature-controlled bath ($\pm$ 0.05°C).

A Kratky camera was used for SAXS measurements. The radiation was Ni-filtered copper (34 kV and 40 mA). Step-scanning was employed the scattered radiation being detected with a proportional counter in conjunction with a pulse height analyser.

3. Results and discussion

3.1. Characterization of the as-quenched structure

The results for the two different liquid-quenching techniques, gun and torsion-catapult, are presented separately. The specimens from the gun technique were directly suitable for X-ray powder studies and for TEM. The torsion-catapult foils were studied with both high-angle X-rays and SAXS. TEM observations were limited to the very thin edges of the foils.

3.1.1. The gun technique

(a) *Lattice parameter – extension of solid solubility.* The gun technique yields a powdery material which is easily removed from the copper substrate. The powder was filtered through a 100 mesh screen and the resulting particles were inserted into a 0.5 mm quartz capillary and mounted in the camera. The patterns were all of good quality and could be measured accurately to 0.01 mm. The lattice parameter obtained from the high angle reflections are extrapolated to $\theta = 90°$ versus the Nelson-Riley function.

The results for the as-liquid-quenched alloys with 20, 40, 70.5% Ag are shown in Fig. 2. The values for the lattice parameters given in Å units were calculated from $K\alpha_1$, $K\alpha_2$ or $K\alpha$ reflections weighted in the ratio 2 to 1. Second-phase lines were detected only in the pattern of the 80% Ag specimen.

The lattice parameter-composition plot shows a negative deviation from Vegard's relation. The

*Unless specified otherwise, all compositions are given in wt %.

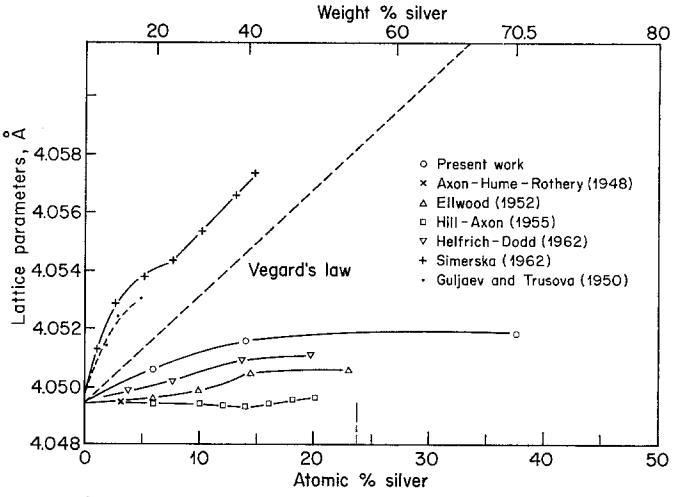

Figure 2 Lattice parameters of liquid quenched Al-Ag alloys compared with the literature values.

lattice parameters of Al-base Ag solid solutions have been the object of several investigations [10-16]. The results are summarized in Table I and plotted together with our results in Fig. 2. The present values of lattice parameters are the highest with the exception of Simerska [16] and Guljaev and Trusova [12]. In both of these studies a positive deviation from Vegard's relation was reported. The values of Simerska were determined at high temperatures and extrapolated to room temperature. The results of Guljaev and Trusova are in question since Pearson [17] has noted that similar measurements by the same authors on systems other than Al-Ag also disagree with different recent work.

If one examines the technique of specimen preparation used by the various investigators, as briefly summarized in Table I, there appears to be a pattern in the results; i.e., the higher the quenching rate, the larger the parameters. Increasing the quenching rate should reduce the amount of quench-clustering. Therefore, it appears that clustering is resulting in a change of lattice parameter, corresponding to a loss of solute from solution. Since lattice parameter increases with solute content, it clearly follows that liquid quenching is superior to bulk quenching in minimizing clustering.

A further observation from the lattice parameter-composition results is that a considerable extension of solid solubility from the 23.7 at. % Ag equilibrium value at high temperature to 37.5 at. % Ag is made possible by liquid quenching. The extension of solid solubility has also been reported by Dixmier and Guinier for this system. Extension of solubility limits in aluminium-base alloys has been observed in numerous studies [18]. As early as 1952, Falkenhagen and Hofmann reported increased solubility for iron, manganese, chromium, vanadium and titanium [19].

(b) *TEM studies.* Large areas of the gun-quenched specimens were adequate for TEM study without thinning. The flakes, easily removed from the copper substrate, were inserted immediately into the electron microscope. The few plates reproduced here are typical of numerous plates which were taken.

Typical microstructures of the Al-20 % Ag are shown in Fig. 3. In all cases a single fcc phase was observed. No unusual selected area diffraction (SAD) patterns were recorded. The grains are elongated – a few microns wide – and the grain boundaries are apparently free of precipitates. Small dislocation loops, 100Å or less in diameter, are seen in Fig. 3b. The change of visibility around the loops is a contrast effect arising when a portion of the loop is steeply inclined to the foil surface. No stacking fault contrast is seen within the loops. Large numbers of dislocations were observed in some areas (Fig. 3c); these may be very irregular helical dislocations. The dislocations seen in Fig. 3c are oriented in a given direction. This area may have been inadvertently deformed during handling. Often, in the thinnest part of the specimen, the area was completely free of any defects. The examination of liquid-quenched Al-40 % Ag gave

TABLE I Lattice parameters of Al-Ag solid solutions

References	Comp. range at. % Ag	Materials	Preparation of specimen	X-ray technique	Calculation	Results
Axon and Hume-Rothery [10]	Up to 6 at. %	99.9945% Al assay Ag	Filings annealed, water quenched	Cu$K\alpha$ radiation Debye-Scherrer in a 19 cm Unicam	N.-R. extrapolation*	No change in lattice spacing could be detected
Dorn *et al* [11]	Up to 0.19 at. %	99.987% Al 99.983% Ag	Filings annealed in pyrex, quenched	Cu$K\alpha$ radiation 10 cm diameter precision focusing camera	N.-R. extrapolation*	No change in lattice spacing could be detected
Guljaev and Trusova [12]	Up to 4.81 at. %	High purity Al ? Ag	Solution-treatment and quenching	Cu$K\alpha$ radiation Powder photograph Sachs camera	?	Lattice spacing increased relatively rapidly with concn and does not agree with other results
Ellwood [13]	Up to 27 at. %	99.9985% Al "spec. pure" Ag	Filings sol. treat. 1 h at 536° C and quenched	Cu$K\alpha$ radiation Powder photograph 9 cm diameter camera	N.-R. extrapolation*	Unchanged by addition of up to 6 at. % between 6 and 14 a small but definite increase, 14 to 27 probably no further increase.
Hill and Axon [14]	Up to 20 at. %	99.991% Al assay Ag	Filings sol. treat. at 560° C and water quenched	Cu$K\alpha$ radiation	*NOTE:* pointed out the importance of quenching rapidly*	Little change or a slight decrease of lattice spacing up to 14 at. % after which the lattice spacing increase.
Helfrich and Dodd [15]	Up to 20 at. %	99.996% Al 99.99+% Ag	Small wires sol treat. 40 h at 540° C, quenched in brine − 20° C	Cu$K\alpha$ radiation	Method of Henry *et al.*	Agree in form with those of Ellwood.
Simerska [16]	Up to 14.55 at. %	99.99% Al 99.9% Ag	Filings	Cu$K\alpha$ radiation High-temperature "Unicam" camera 19 cm diameter	Extrapolation from high-temperature	Clear increase with silver concentration.
Present work	Up to 37.5 at. %	99.999% Al 99.99% Ag	Particles < 100 mesh in 0.5 mm capillary liquid quench	Cu$K\alpha$ radiation Debye-Scherrer 19 cm diameter	N.-R. extrapolation	See text

*Values given in kX converted to Å units.

Figure 3(a) to (c). Typical electron micrographs of as liquid-quenched (gun technique) Al-20% Ag.

similar results: a single phase and elongated grains. There appears to be no influence of concentration on grain size.

Examples of micrographs for the eutectic composition, Al-70.5% Ag, are seen in Fig. 4. Even for the thinnest sections (a) and (b), the grain boundaries contain some form of precipitate. A second phase is present in (c). The apparent periodic alignment of this precipitate may be due to the nearly unidirectional heat transfer during solidification. A dendritic-type structure is also observed for the Al-80% Ag alloy (Fig. 5). The characteristic tree-like pattern in micrograph (a) has a spacing of approximately 1200 to 1600Å. Larger spacings are visible in the thicker areas of Fig. 5.

Dendrite arm spacing is a function of the rate of cooling [20] and, therefore, can be used to estimate quenching rate [21]. Using the expression of Chalmers [20] and the data of Matyja *et al* [21], it is found that the cooling rate for the present experiments is of the order of 10^6 °C sec^{-1}, which is in good agreement with previous estimates for the gun technique [4].

3.1.2. The torsion-catapult

High-angle X-ray diffraction patterns were taken from both surfaces of a number of liquid-quenched foils. The surface finish of the copper substrate was found to have a noticeable influence on the patterns. If a sand-blasted substrate was used, no distinction between the two surfaces (i.e. the specimen surface in contact with the substrate versus the surface exposed to the atmosphere) could be made on the basis of the diffraction patterns for the low concentration alloys. On the other hand, for the high concentration alloys, if a polished surface was used, the presence of a second phase was observed on the side of the foil not in contact with the substrate.

The TEM results for the torsion-catapult are similar to the observations made using the gun

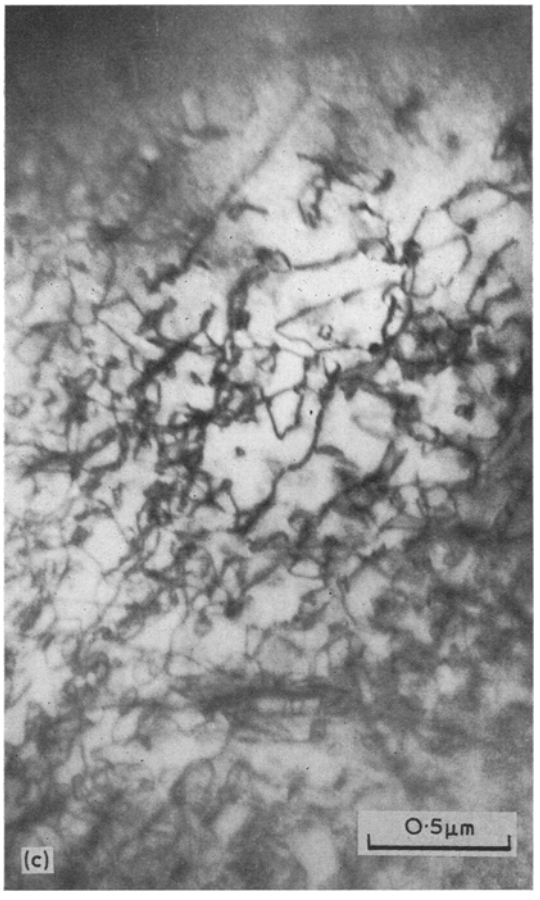

Figure 3 continued.

technique. Large numbers of small dislocation loops and helical dislocations are observed. A plane of zero contrast is seen for some of the loops, indicating a large inclination of the invisible segment to the foil surface. Where dislocations exist, the density of loops is greatly reduced or even totally absent. A single fcc phase was obtained for Al-20% Ag and Al-40% Ag.

3.1.3. *Efficiency of the liquid quench*

X-ray powder patterns and TEM results indicate that for a wide composition range solid solutions can be obtained by quenching from the liquid. However, both normal X-ray methods and TEM are relatively insensitive to decomposition on a very small scale. Heterogeneities of 20Å or less are difficult to detect with TEM – especially so in Al-Ag due to the absence of any strain contrast. SAXS studies were undertaken to study small-scale clustering in an effort to compare the efficiency of the liquid quenching technique with normal solid quenching.

The interpretation of many of the SAXS data involved the determination of the radius of gyration (Appendix 1). In the present study it was often observed that the Guinier plots ($\log I$ versus ϵ^2) were not linear over the entire angular range of interest, indicating that the system contains a significant distribution of particle sizes. Jellinek *et al* [22] have suggested a graphical method for analysing such data. The approach is straightforward and provides useful qualitative information. In this method the particle size distribution is approximated by a set of discrete fractions. The method was applied to both solid-quenched specimens and to specimens quenched from the liquid onto substrates of different surface conditions.

The results of this graphical analysis of the SAXS data are given in Table II and lead to some interesting conclusions. For the solid-quenched specimens, large particles (> 21Å) account for a considerable weight fraction (40%). On the other hand, quenching from the liquid onto a substrate with good heat transfer produces a rather sharp particle size distribution: small particles, 12 to 13Å diameter, represent over 95% of the weight fraction. Particle size distribution is considerably narrower for the polished (320 grit) surface. Note too that substrate temperature has a much smaller influence than surface finish condition.

TABLE II Summary of SAXS calculations

Condition	Particle radius (Å)	Weight fraction
Solid-quenched		
550°C → brine (− 22°C)	7.5	0.60
	21.0	0.25
	27.0	0.15
Liquid-quenched		
1. Substrate ground 320 grits,	8.0	0.56
temperature 40°C	18.5	0.15
	26.5	0.29
2. Substrate sand-blasted,	6.5	0.96
temperature 40°C	15.0	0.04
3. Substrate sand-blasted,	5.5	0.95
temperature 12°C	13.5	0.05

3.2. Decomposition of the liquid-quenched structures

Following the analysis of the as-quenched

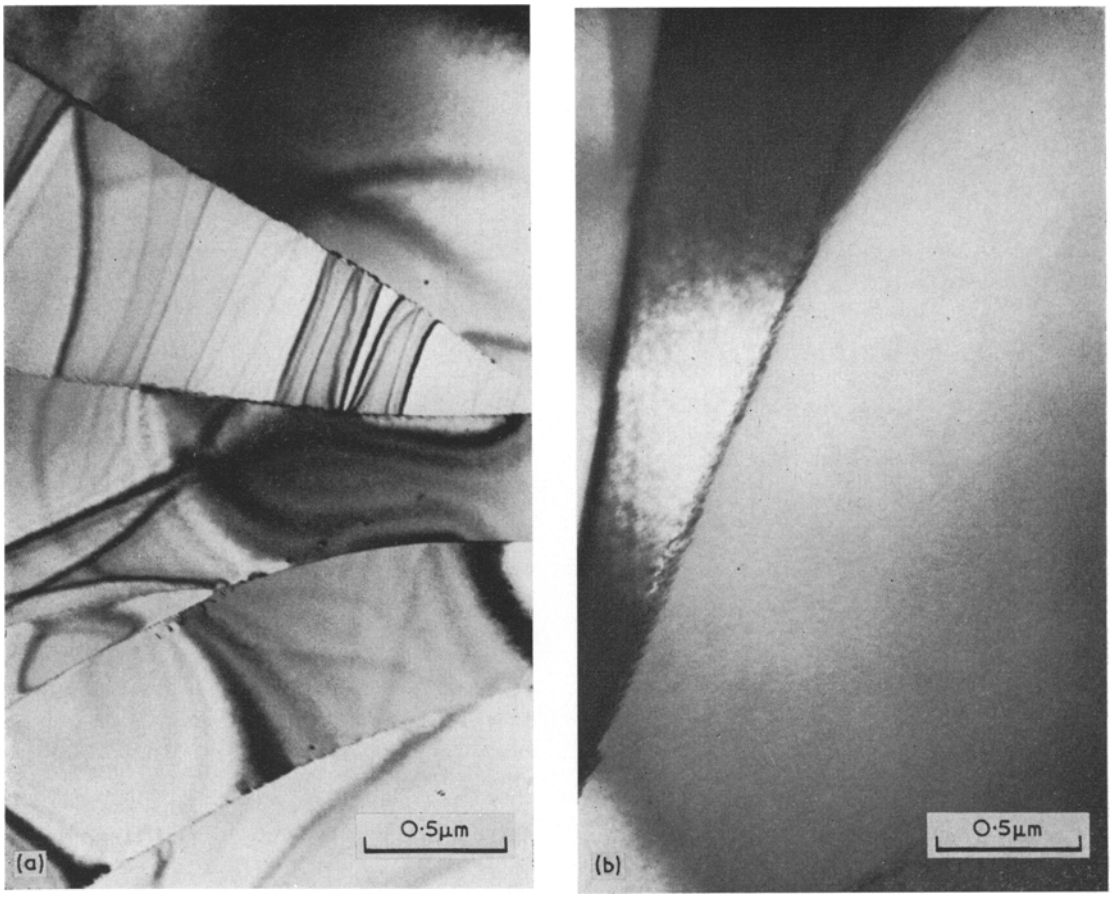

Figure 4(a) to (c). Typical electron micrographs of as liquid-quenched (gun technique) Al-70.5% Ag.

condition, the decomposition of the liquid-quenched specimens was investigated both kinetically and microstructurally. The observation of decomposition in specimens prepared using the gun technique was limited to hot-stage TEM. The torsion-catapult specimens were investigated using electrical resistance, high-angle X-rays and SAXS. The decomposition was followed in the temperature range from 50 to 200°C.

3.2.1. Gun technique, hot-stage TEM

Direct micrographic evidence of precipitation in thin sections of liquid-quenched Al-40% Ag specimens is shown in Fig. 6. The as-quenched structure is shown in Fig. 6a, where a solid solution with a small amount of grain-boundary precipitate is observed. The temperature of the hot stage was estimated to be 300°C. No photograph could be taken during the first 5 min because of thermal drifting of the image. The structure after 5 min (Fig. 6b) has two characteristic features: copious precipitation is observed along grain boundaries and, in some grains, long narrow precipitates, γ' or γ, are seen. The background structure is initially without distinct shape or morphology, but appears to be a non-oriented modulated precipitate. The modulations* grow competitively except near the growing γ' precipitates or near grain boundaries. The modulated structure is seen to mature, changing gradually to individual particles. The maximum observed dimension of these particles is about 500Å, as seen in Fig. 6e. Those particles within

*The size of the background modulations is difficult to estimate. The measurements were always made in the same region in each micrograph where the influence of grain boundaries and precipitates are the least. A line was traced at random and the number of modulations or particles of different shade were counted. A linear dependence of dimension on time is found when the particle size is plotted as a function of ageing time on a log-log scale.

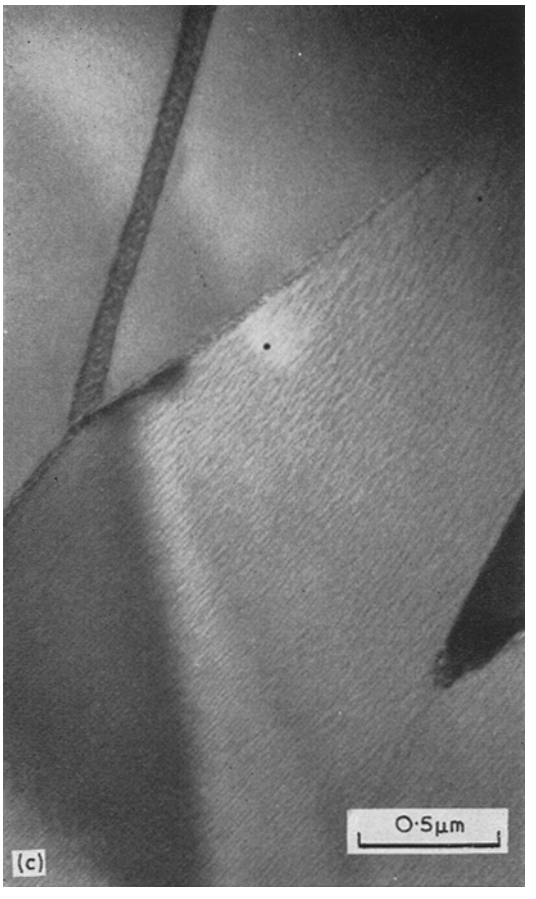

Figure 4 continued.

the grains dissolve in regions adjacent to growing platelets or grain boundaries.

3.2.2. Torsion-catapult technique

The electrical resistance of liquid-quenched Al-40% Ag was measured at room temperature by the interruption of isothermal ageing in the temperature range 110 to 175°C (Fig. 7). In addition, a kinetic study of ageing was carried out at 150 and 175°C with high-angle X-ray diffractometry. A second phase, indexed as hcp, develops on ageing in this temperature range. The integrated intensities of the (1.01) reflection of the second phase and the (200) matrix reflection were measured as a function of time at 150 and 175°C. The intensity of the (1.01) reflection increases with ageing time while the (200) matrix reflection decreases.

An empirical analysis is used to describe the isothermal kinetics for both the resistance and the X-ray experiments. The early regime of many solid-state isothermal reactions can be described by a form of the Johnson-Mehl equation:

$$\log \ln \left(\frac{1}{1-X}\right) = \log K + n \log t \quad (1)$$

where X is the fraction transformed at time t, K

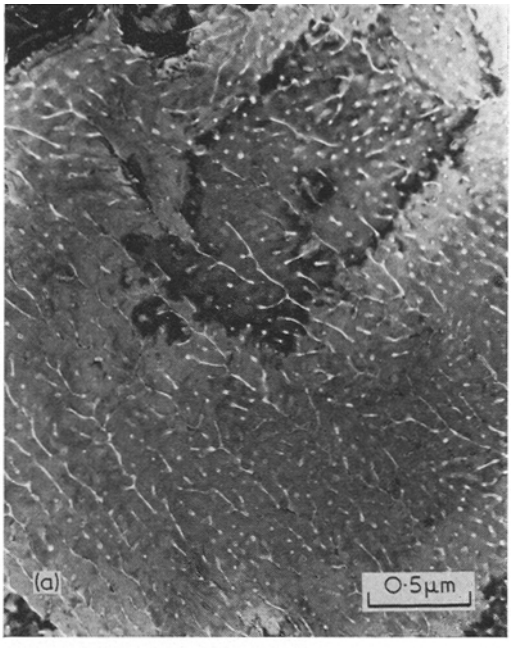

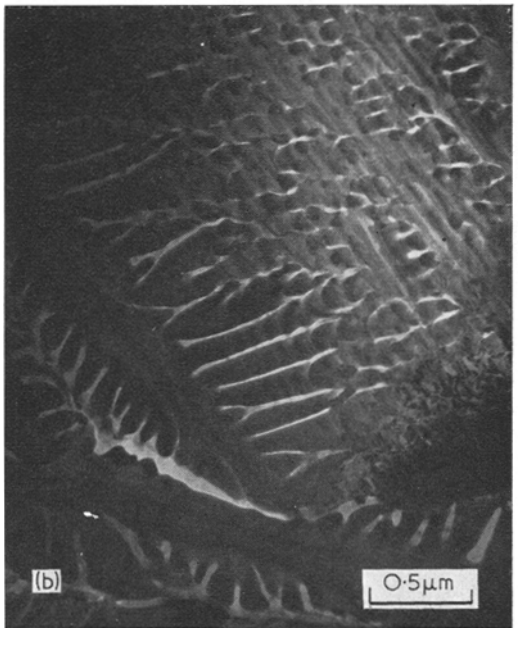

Figure 5(a) and (b) Typical electron micrographs of as liquid-quenched (gun technique) Al-80%. Ag.

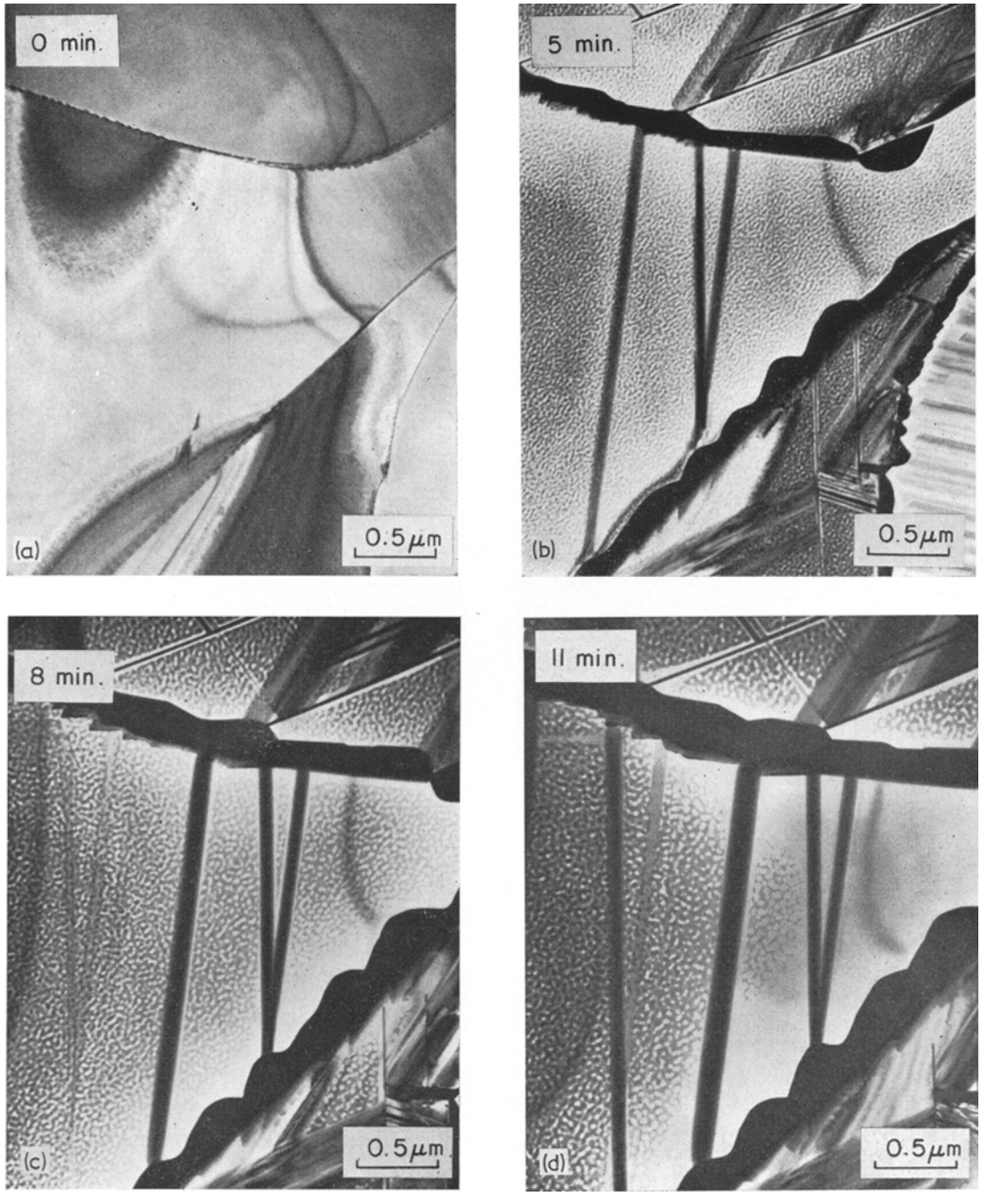

Figure 6(a) to (f). Electron micrographs sequence from liquid-quenched Al-40% Ag aged in the microscope (gun technique).

is a temperature-dependent parameter containing the activation energy for the process, and n is a constant. X can be related to a change in property by

$$X = \frac{P_0 - P_t}{P_0 - P_\infty} \tag{2}$$

where the subscripts are for zero time, time t and

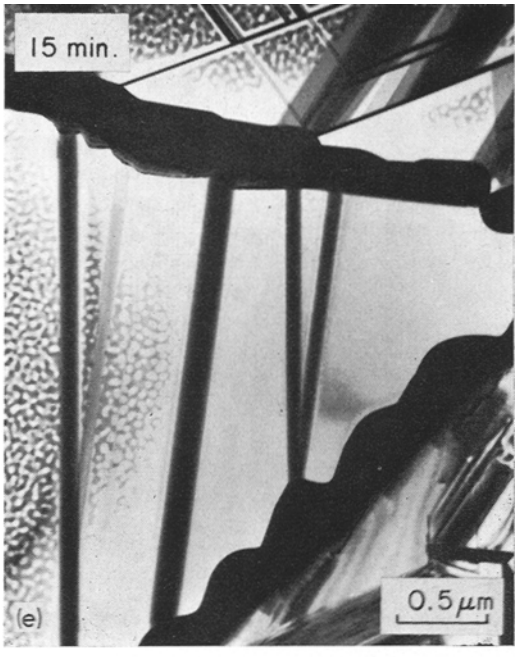

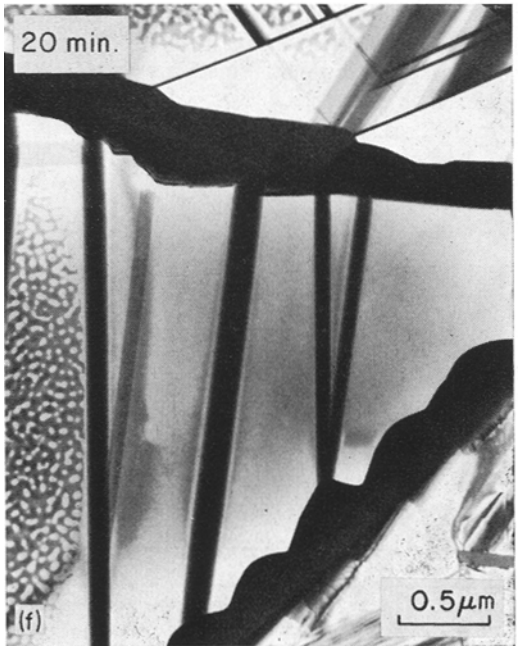

Figure 6 continued.

infinity, respectively [23]. The properties used here are electrical resistance, R, and integrated X-ray intensity of a given reflection. An activation energy, Q, for the process can be computed

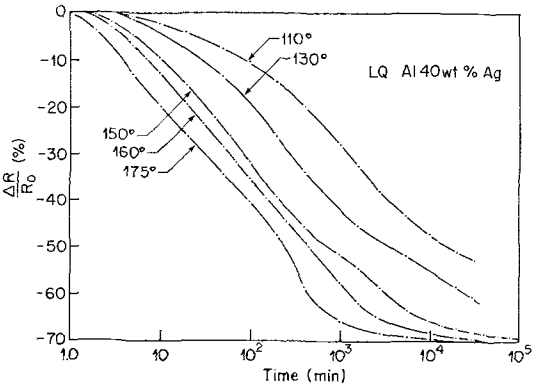

Figure 7 Change in electrical resistance versus time for liquid-quenched Al-40% Ag aged at 110, 130, 150, 160 and 175°C (torsion-catapult).

from the experimental data in a number of ways; rate-constant method, cross-cut method and change-of-slope method.

To test Equation 1, the appropriate plot for ageing at 175°C is shown in Fig. 8 and consists of two linear sections of slopes 1.6 and 0.5, respectively. The plots for ageing at 150 and 160°C are similar but exhibit larger deviations from linearity. The fraction transformed versus ageing time as determined from X-ray data is shown in Fig. 9; data for two ageing temperatures are included.

The activation energies determined by the three methods from the electrical resistance and X-ray data are reported in Table III together with the evaluation of n.

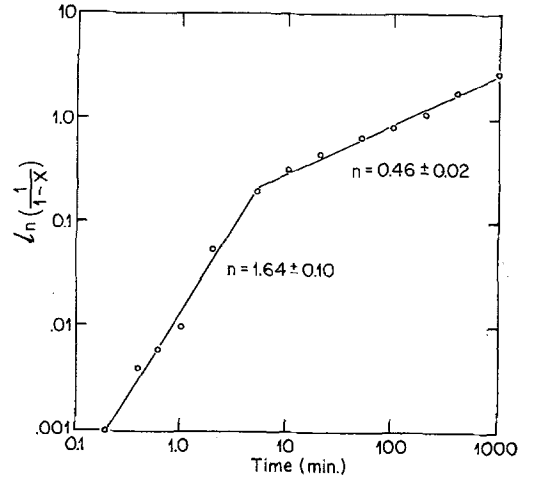

Figure 8 log ln(1/1 − X) versus log t plot from analysis of change in resistance data (ageing at 175 °C).

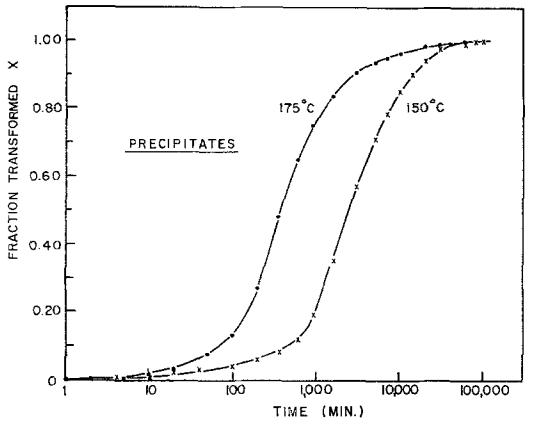

Figure 9 Fraction transformed as a function of ageing time at 150 and 175°C evaluated from the intensity change of the (1.01) reflection.

Consider first the evaluation of n. Two values are obtained in the temperature range 150 to 175°C. The first stage has an n of 1.6 which extends to 0.18 fraction transformed; the second stage with an n of 0.5 extends from 0.18 to about 0.93 fraction transformed. On the other hand, for the X-ray study at 150°C a similar analysis gives an n of 0.5 for a short initial portion extending up to 0.08, followed by a value near unity up to 0.57 fraction transformed. At 175°C a single stage is observed with an n of unity from 0.02 to 0.65 fraction transformed.

It is of interest to compare these experimentally determined values of n with theory. Ham [24] has shown that a value for n of 3/2 is characteristic of the diffusion-controlled growth of a fixed number of particles irrespective of the shape of the particles. For thickening of large plates by diffusion, n is expected to be 1/2. The values of n obtained from the change in resistance can thus be explained by initial diffusion-controlled growth of particles, followed by a stage of thickening of the precipitate platelets.

The changes in intensity of the precipitate and matrix X-ray reflections give a value of unity for n which is not consistent with the resistance data. A comparison between the isothermal ageing at 175°C for the resistance and X-rays (cf. Figs. 7 and 9) indicates for the former that the time for half-reaction is about 80 min, whereas it is about 700 min for the X-ray data. It is thus clear that the X-ray data represent a later feature of the reaction. The unity value found for n at 175°C from the X-ray data is likely due to coarsening: the scattered X-ray intensity will change with volume of the growing phase, and in coarsening reactions the average radius grows as $t^{1/3}$. The volume will thus grow as t, which is observed from the X-ray data at 175 and at 150°C after an $n = \frac{1}{2}$ transient.

TABLE III Summary of the empirical kinetics analysis

Evaluation of n

Temperature range (°C)	Electrical resistance	High-angle X-ray diffraction
150 to 175	1.64 ± 0.10 $(X = 0.00 \rightarrow 0.18)$ 0.46 ± 0.02 $(X = 0.18 \rightarrow 0.98)$	
150		0.48 ± 0.02 $(X = 0.01 \rightarrow 0.08)$ 1.12 ± 0.06 $(X = 0.08 \rightarrow 0.57)$
175		1.00 ± 0.03 $(X = 0.02 \rightarrow 0.65)$

Activation energies in kcal mol^{-1}

Method	Temperature range (°C)	Electrical resistance	High-angle X-ray
Rate-constant	110 to 175	20.0 ± 1.7	—
	150 to 175	—	27.5 ± 2.2
Cross-cut	110 to 175	Increases up to $X = 0.3$, then 19.6	—
	150 to 175	—	Decreases up to $X = 0.2$, then 26.8
Change-of-slope	110 to 175	19.7 ± 1.0	—

Let us now consider the multiple values of activation energies, Q, obtained from the resistance and the X-ray data (Table III). Of the three methods used, the rate-constant and cross-cut methods are closely connected since the rate is simply an evaluation of Q at 0.632 fraction-transformed. Any variation of Q with X is best observed using the change-of-slope method. The value obtained at a certain fraction transformed, X, using the cross-cut technique, is an average of the process from the beginning to the value under consideration.

The estimate of Q for the total temperature range under investigation by the three methods of calculation using the resistance data, agree well with an average value of 19.6 ± 1.0 kcal mol^{-1}. The estimate is also found to be nearly independent of the fraction-transformed. Our value is close to the results of Turnbull *et al* [25] and Borelius and Larsson [26] using electrical resistance and Baur and Gerold [27] using SAXS.

The apparent activation energy which is obtained from the X-ray study is noticeably different. The rate-constant estimate is 27.5 ± 2.2 kcal mol^{-1}. Using the cross-cut method, the value of 32.3 ± 2.5 kcal mol^{-1} obtained at $X = 0.1$ rapidly decreases and reaches a plateau of 26.9 ± 1.4 kcal mol^{-1} from $X = 0.2$ to 0.7. These energies are close to the value of Toman, 28.6 kcal mol^{-1}, for a similar study on single crystal Al-9.6 at. % Ag aged in the temperature range 173 to 260°C [28]. Köster and his group, following changes in physical properties, also give a similar value for the activation energy [29].

In summary, two activation energies are observed in the temperature range 110 to 175°C; approximately 20 ± 2 kcal mol^{-1} from the change in electrical resistance and 27 ± 2 kcal mol^{-1} from the high-angle X-ray study. The latter is probably representative of equilibrium volume diffusion, and the good agreement with the activation energy results from the single-crystal study of Toman eliminates grain-boundary diffusion as an important factor.

Since the resistivity data are representative of an earlier stage of reaction than for the X-ray measurements the lower activation energies noted for the former can be explained as being due to liquid-quenched excess vacancies. The original quench will freeze in large numbers of excess vacancies (certainly the system contains of the order of 10^{-4} atomic fractions vacancies prior to the quench). Some of the vacancies persist in metastable traps and are likely released and are available for enhancing the precipitation reaction. This enhancement is observed in the resistivity data, but not in the X-ray studies, where mainly later, post-vacancy decay reactions predominate. This is consistent with the values of n which were obtained in this study.

4. Conclusions

It has been possible to quench a wide range of Al-Ag alloys into regions of the phase diagram not accessible by solid quenching. Electrical resistivity, X-ray techniques and TEM have been used to characterize the as-quenched condition and to follow the kinetics, structures and morphologies of the decomposition products of the liquid-quenched specimens.

4.1. The gun technique

Lattice parameter measurements indicate that liquid-quenching is superior to bulk-quenching in minimizing clustering.

Considerable extension of solid solubility, from the 55.6% Ag (23.7 at. % Ag) equilibrium limit to 70.5% Ag (37.5 at. % Ag), is made possible by liquid-quenching.

In typical microstructures of the low-concentration alloys (20 and 40% Ag) the grains are elongated and the grain boundaries are free of precipitates. In the highly concentrated Al-80% Ag alloy a dendritic-type structure is observed and, using the dendrite arm spacing, the cooling rate is found to be of the order of 10^6 °C sec^{-1}.

The observation of decomposition of Al-40% Ag was carried out with hot-stage TEM at 300°C. The structure after a few minutes at temperature had some characteristic features; copious precipitation along the grain boundaries, long narrow precipitates of γ' or γ within some of the grains and background composition modulations. These modulations developed and grew competitively to a maximum dimension of about 500Å. It is suggested that the modulations are a manifestation of spinodal decomposition. A SAXS study supporting this conclusion will be reported in a forthcoming publication [30].

4.2. The torsion-catapult technique Al-40% Ag

The TEM results are similar to the observations made on the specimens from the gun technique.

The sharper size distribution of the clusters, as

obtained from SAXS, confirm that liquid-quenching is more efficient than bulk-quenching in preserving a solid solution.

The time law exponent, n, and the activation energy, Q, of the empirical analysis were evaluated for the electrical resistance and X-ray data. The values of n obtained from the change in resistance can be explained by initial diffusion-controlled growth of particles followed by a stage of thickening of the precipitate platelets. On the other hand, the X-rays are sensitive principally to a later feature of the reaction, and the value of unity found for n is likely due to coarsening.

Two activation energies are observed in the temperature range 110 to 175°C; approximately 20 ± 2 kcal mol^{-1} from the change in electrical resistance and 27 ± 2 kcal mol^{-1} from the X-ray study. The latter is representative of equilibrium volume diffusion, while the lower Q noted for the resistance data can be due to liquid-quenched excess vacancies.

Acknowledgements

This study was carried out in partial fulfilment for the Ph.D. degree of R.R. at the University of Pennsylvania. This research was supported at the University of Pennsylvania by the Advanced Research Projects Agency of the Department of Defense and at the State University of New York by the US Army Research Office, Durham.

Appendix 1

Guinier*, assuming that the particles are of identical shape, sufficiently well-spaced and of random distribution, has shown that the intensity of the scattered X-rays can be approximated by,

$$I = Mn^2 I_e \exp\left(-\frac{4\pi^2 R^2 \epsilon^2}{3\lambda^2}\right)$$

where M = the number of scattering particles irradiated; n = the difference in the number of electrons between the particle and the surrounding matrix; R = radius of gyration; I_e = the intensity scattered by an electron; ϵ = the scattering angle = 2θ; λ = the wavelength of the X-rays. As seen from the equation, if the logarithm of the scattered intensity is plotted versus the square of the scattered angle, the slope of the line can be used to determine the radius of gyration, R.

References

1. A. KELLY and R. B. NICHOLSON, *Prog. Mater. Sci.* **10** no. 3 (1963).
2. R. BAUR and V. GEROLD, *Acta Metallurgica*, **10** (1962) 637.
3. P. DUWEZ, *Prog. Solid State Chem.* **3** (1966) 377.
4. *Idem, Trans. ASM* **60** (1967) 606.
5. B. C. GIESSEN, Proceedings of the 12th Sagamore Army Materials Research Conference, Syracuse University Press (1966).
6. T. R. ANANTHARAMAN and C. SURYANARAYANA, *J. Mater. Sci.* **6** (1971) 1111.
7. P. FURRER and H. WARLIMONT, *Z. Metallk.* **62** (1971) 12; **62** (1971) 100.
8. R. ROBERGE and H. HERMAN, *Mater. Sci. and Eng.* **3** (1968/69) 62.
9. P. DUWEZ and R. H. WILLENS, *Trans. Met. Soc. AIME* **227** (1963) 362.
10. H. J. AXON and W. HUME-ROTHERY, *Proc. Roy. Soc. (London)* **193** (1948) 1.
11. J. E. DORN, P. PIETROKOWSKY, and T. E. TIETZ, *Trans. Met. Soc. AIME* **188** (1950) 933.
12. A. P. GULJAEV and E. F. TRUSOVA, *Structure Reports* **13** (1950) 6.
13. E. C. ELLWOOD, *J. Inst. Metals* **80** (1951-52) 605.
14. R. B. HILL and H. J. AXON, *Research* **8** (1955) S2.
15. W. J. HELFRICH and R. A. DODD, *Trans. Met. Soc. AIME* **224** (1962) 757.
16. M. SIMERSKA, *Czech. J. Phys.* **12** (1962) 54.
17. W. B. PEARSON, "A Handbook of Lattice Spacings and Structures of Metals and Alloys", Vol. 1 (Pergamon Press, New York, 1958).
18. J. DIXMIER and A. GUINIER, *Mém. Scient. Rev. Métall* **64** (1967) 53.
19. G. FALKENHAGEN and W. HOFMANN, *Z. Metallk.* **43** (1952) 69.
20. B. CHALMERS, "Principles of Solidification" (John Wiley, New York, 1964).
21. H. MATYJA, B. C. GIESSEN, and N. J. GRANT, *J. Inst. Metals* **96** (1968) 30.
22. M. H. JELLINEK, E. SOLOMON, and I. FANKUCHEN, *Ind. Eng. Chem. Anal. Ed.* **18** (1946) 172.
23. M. E. FINE, "Phase Transformations in Condensed Systems" (Macmillan, New York, 1964).
24. F. S. HAM, *J. Phys. Chem. Solids* **6** (1958) 335.
25. D. TURNBULL, H. S. ROSENBAUM, and H. N. TREAFTIS, *Acta Metallurgica* **8** (1960) 277.
26. G. BORELIUS and L. E. LARSSON, *Arkiv. för Fysik* **11** (1956) 137.
27. R. BAUR and V. GEROLD, *Z. Metallk.* **52** (1961) 671.
28. K. TOMAN, *Czech. J. Phys.* **9** (1959) 367.
29. W. KÖSTER and F. SPERNER, *Z. Metallk.* **44** (1953) 217.
30. R. ROBERGE and H. HERMAN, *Fizika* **2** (1970) 6.1, and R. ROBERGE and H. HERMAN, in preparation.

Received 20 March and accepted 22 March 1973.

*A. Guinier and G. Fournet, "Small-Angle Scattering of X-rays" (John Wiley, New York, 1955).